Facile One-Step Synthesis and Transformation of Cu(I)-Doped Zinc Sulfide Nanocrystals to Cu1.94S-ZnS Heterostructured Nanocrystals

ARTICLE *in* LANGMUIR · JUNE 2013

Impact Factor: 4.46 · DOI: 10.1021/la401707u · Source: PubMed

9 AUTHORS, INCLUDING:

Yanbing Hou
Beijing Jiaotong University
114 PUBLICATIONS **1,599** CITATIONS
SEE PROFILE

Hongshang Peng
Minzu University of China
48 PUBLICATIONS **1,165** CITATIONS
SEE PROFILE

Fujun Zhang
Beijing Jiaotong University
208 PUBLICATIONS **1,420** CITATIONS
SEE PROFILE

Feng Teng
Beijing Jiaotong University
224 PUBLICATIONS **1,561** CITATIONS
SEE PROFILE

Langmuir

Article

pubs.acs.org/Langmuir

Facile One-Step Synthesis and Transformation of Cu(I)-Doped Zinc Sulfide Nanocrystals to $Cu_{1.94}S$–ZnS Heterostructured Nanocrystals

Haihang Ye,[†] Aiwei Tang,*[,†,‡] Liming Huang,[†] Yu Wang,[†] Chunhe Yang,[†] Yanbing Hou,[‡] Hongshang Peng,[‡] Fujun Zhang,[‡] and Feng Teng*[,‡]

[†]Department of Chemistry and [‡]Key Laboratory of Luminescence and Optical Information, Ministry of Education, Beijing JiaoTong University, Beijing 100044, P. R. China

Supporting Information

ABSTRACT: A facile one-pot heating process without any injection has been developed to synthesize different Cu–Zn–S-based nanocrystals. The composition of the products evolves from Cu(I)-doped ZnS (ZnS:Cu(I)) nanocrystals into heterostructured nanocrystals consisting of monoclinic $Cu_{1.94}S$ and wurtzite ZnS just by controlling the molar ratios of zinc acetylacetonate ($Zn(acac)_2$) to copper acetylacetonate ($Cu(acac)_2$) in the mixture of *n*-dodecanethiol (DDT) and 1-octadecene (ODE). Accompanying the composition transformation, the crystal phase of ZnS is changed from cubic zinc blende to hexagonal wurtzite. Depending on the synthetic parameters including the reaction time, temperature, and the feeding ratios of Zn/Cu precursors, the morphology of the as-obtained heterostructured nanocrystals can be controlled in the forms of taper-like, matchstick-like, tadpole-like, or rod-like. Interestingly, when the molar ratio of $Cu(acac)_2$ to $Zn(acac)_2$ is increased to 9:1, the crystal phase of the products is transformed from monoclinic $Cu_{1.94}S$ to the mixed phase composed of cubic $Cu_{1.8}S$ and tetragonal $Cu_{1.81}S$ as the reaction time is further prolonged. The crystal-phase transformation results in the morphological change from quasi-spherical to rice shape due to the incorporation of Zn ions into the $Cu_{1.94}S$ matrix. This method provides a simple but highly reproducible approach for synthesis of Cu(I)-doped nanocrystals and heterostructured nanocrystals, which are potentially useful in the fabrication of optoelectronic devices.

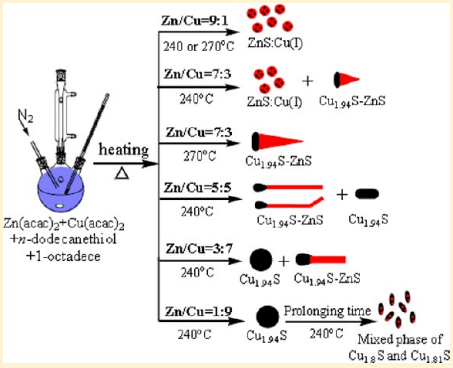

1. INTRODUCTION

Semiconductor nanocrystals have been intensively studied in the past few decades from fundamental research to practical applications in light-emitting diodes, photovoltaic cells, biological labels, and so on.[1−6] To meet the growing demand of the applications in optoelectronic devices and biological technology, different types of semiconductor nanocrystals, such as doped, alloyed, and heterostructured nanocrystals, have been developed in recent years.[7−12] In particular, enormous efforts have been devoted to preparing semiconductor nanocrystals doped with different metal and various semiconductor heterostructured nanocrystals consisting of two or more components within one particle. Incorporation of different atoms or ions into host materials entitles these doped nanocrystals novel properties and functions, while retains most of the advantages of the host materials. It is worth mentioning that the doped semiconductor nanocrystals can avoid the self-quenching due to their substantial ensemble Stokes shift, and they are insensitive to thermal and photochemical disturbances.[13−16] Very recently, the doped semiconductor nanocrystals are thus regarded as a lucrative alternative to semiconductor nanocrystals. Elaboration of multicomponent semiconductor heterostructured nanocrystals endows them with diverse functionalities or unique properties through construction of semiconductor–metal or semiconductor–semiconductor heterojunctions with different building blocks, which are very promising in the fields of photovoltaic cells, biomedical sensing, and a new generation of optoelectronic devices.[17−25] Therefore, to design and construct multifunctional semiconductor heterostructured nanocrystals has been a key aim of material scientists.

To date, a variety of approaches have been developed to prepare doped or heterostructured semiconductor nanocrystals. The most popular one is wet-chemistry approaches, in which the shape, crystal phase, and the composition of the products can be controlled by careful regulation of thermodynamic parameters and growth kinetics in solution phase with the assistance of the selected surfactants and ligands.[11,26−28] For example, the typical hot-injection strategy can yield high-quality doped or heterostructured nanocrystals based on simultaneous burst of nucleation and well-controlled growth.[28−34] However, such a method is limited by reproducibility, high toxicity, and large-scale production.[29,35] Therefore, an alternative approach is desired for less toxic and more convenient control.

Lately, Gao's group first demonstrated that $Cu_{1.94}S$ nanocrystals were used as catalysts for preparing one-dimensional

Received: May 6, 2013
Revised: June 15, 2013
Published: June 15, 2013

heterostructured nanocrystals with different morphologies.[12,20] Thereafter, various $Cu_{1.94}S$-based heterostructured semiconductor nanocrystals with different components have been successfully synthesized using different solution-processed approaches, including hexagonal-prismatic $Cu_{1.94}S$–ZnS, disk-like $C_{1.94}S$–CdS, and cylindrical Cu_2S–PbS.[19,36,37] Until now, however, few works about the synthesis of ZnS:Cu(I) nanocrystals and $Cu_{1.94}S$–ZnS heterostructured nanocrystals in the same reaction system have been reported. Herein, we present a facile one-pot colloidal route for synthesis of ZnS:Cu(I) nanocrystals and $Cu_{1.94}S$–ZnS heterostructured nanocrystals by thermal decomposition of $Zn(acac)_2$ and $Cu(acac)_2$ in the mixture of DDT and ODE. By adjusting molar ratios of $Zn(acac)_2$ to $Cu(acac)_2$, the as-obtained products could be transformed from ZnS:Cu(I) nanocrystals to $Cu_{1.94}S$–ZnS heterostructured nanocrystals, and the crystal phase of ZnS is changed from cubic zinc blende to hexagonal wurtzite accordingly. Moreover, when the molar ratio of $Cu(acac)_2$ to $Zn(acac)_2$ is increased to 9:1, a mixed phase of cubic $Cu_{1.8}S$ and tetragonal $Cu_{1.81}S$ can be obtained as the reaction time is prolonged; meanwhile, the morphology is changed from spherical to rice shape.

2. EXPERIMENTAL SECTION

Sample Synthesis. For a typical synthesis of ZnS:Cu(I)-doped nanocrystals, 4.5 mmol of $Zn(acac)_2$ and 0.5 mmol of $Cu(acac)_2$ were mixed with 5 mL of DDT and 15 mL of ODE in a three-neck flask and then degassed using N_2 flow under magnetic stirring for about 20 min. The mixture was then heated slowly to 240 °C for a fixed time. Afterward, the reaction was terminated by cooling down to room temperature naturally after removal of the heating source. The product was purified by three repeated actions of dissolving the precipitate in chloroform and then reprecipitating by adding excess ethanol. Finally, the resultant sample was redissolved into chloroform or dried in vacuum for further characterization. Other samples were synthesized with similar procedures except the molar ratios of $Zn(acac)_2$ to $Cu(acac)_2$, or the reaction temperature was changed while the overall amount of $Zn(acac)_2$ and $Cu(acac)_2$ was kept at 5 mmol. The product constituent of the final products together with the experimental conditions are denoted as samples A–H and summarized in Table 1. It should be noted that the doped and heterostructured nanocrystals are synthesized just by controlling the molar ratios of $Zn(acac)_2$ to $Cu(acac)_2$.

Sample Characterizations. The transmission electron microscopy (TEM) images of the resultant nanocrystals were characterized on a JEM-1400 transmission electron microscope operating at an accelerating voltage of 100 kV. High-resolution TEM images were taken on a JEM-2010 at an acceleration voltage of 200 kV. Powder X-ray diffraction (XRD) patterns were obtained by using a Bruker D8 Advance diffractometer using a Cu Kα radiation source (λ = 1.540 56 Å). X-ray photoelectron spectroscopy (XPS) measurement was performed on a VG ESCALAB 220i-XL spectrometer with a 300 W Al Kα radiation source. All binding energies for different elements were calibrated with respect to C 1s line at 284.8 eV from the contaminant carbon. UV–vis–NIR absorption spectra were performed on a Varian 5000 spectrophotometer.

Table 1. Experimental Conditions for Synthesis of Different Products and the Corresponding Results

samples	$Zn(acac)_2$ (mmol)	$Cu(acac)_2$ (mmol)	reaction temp (°C)	products
A	5	0	240	ZnS
B	4.5	0.5	240	ZnS:Cu(I)
C	4.5	0.5	270	ZnS:Cu(I)
D	3.5	1.5	240	ZnS:Cu(I) and a few of $Cu_{1.94}S$–ZnS heterostructures
E	3.5	1.5	270	$Cu_{1.94}S$–ZnS heterostructures
F	2.5	2.5	240	$Cu_{1.94}S$–ZnS heterostructures
G	1.5	3.5	240	Cu_2S and $Cu_{1.94}S$–ZnS heterostructures
H	0.5	4.5	240	mixed phase of $Cu_{1.81}S$ and $Cu_{1.8}S$

3. RESULTS AND DISCUSSION

Synthesis of ZnS:Cu(I) Nanocrystals. As a control experiment, pure ZnS nanocrystals can be obtained by direct heating 5 mmol of $Zn(acac)_2$ in the mixture of DDT (5 mL) and ODE (15 mL). In this case, DDT acts as a reactive solvent but mainly as a sulfur source and a surface-capping agent, while ODE as a solvent to allow the reaction to take place at a high temperature. The XRD patterns of the as-obtained ZnS nanocrystals shown in Figure 1 indicate that the products possess a cubic zinc blende structure, and the three major diffraction peaks can be assigned to (111), (220), and (331) planes according to the standard patterns of the cubic ZnS (JCPDS No. 80-0020). When 0.5 mmol of $Cu(acac)_2$ was added into the reaction system while the amount of $Zn(acac)_2$ was reduced to 4.5 mmol, the XRD patterns of the products obtained at 240 and 270 °C shown in Figure 1 display three obvious diffraction peaks similar to those of cubic ZnS nanocrystals, respectively. No characteristic peaks of Cu-related impurity are detected in the XRD patterns, indicating that the Cu ions are successfully doped into the ZnS lattices, which is in agreement with our previous report.[7] The broadening of XRD peaks of the three samples indicates the nature of small size. The corresponding TEM images of samples A–C shown in Figure 2 demonstrate that the average size is less than 5 nm with an irregular shape.

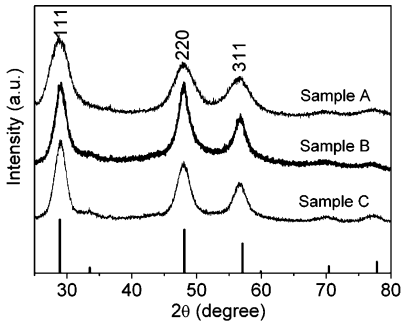

Figure 1. XRD patterns of samples A–C with the lines at the bottom lines from cubic zinc blende ZnS (JCPDS No. 80-0020).

In order to reveal the details on the valence state of the Cu ions and the chemical composition of the sample, XPS analysis was performed. We take sample C as an example, and the detailed results are shown in Figure 3. A survey XPS spectrum of sample C presented in Figure 3a reveals the presence of Zn, Cu, and S in the as-obtained product. The high-resolution spectrum of the Cu 2p signal shown in Figure 3b displays two peaks at 952.4 and 932.5 eV, corresponding to the characteristic Cu $2p_{1/2}$ and Cu $2p_{3/2}$ of Cu(I).[7] No "shake-up" peaks are observed between the Cu $2p_{3/2}$ and Cu $2p_{1/2}$, which rules out the possibility of Cu^{2+} in our samples according to previous reports.[38,39] The Zn 2p peaks located at 1044.7 and 1021.7 eV

dx.doi.org/10.1021/la401707u | Langmuir 2013, 29, 8728–8735

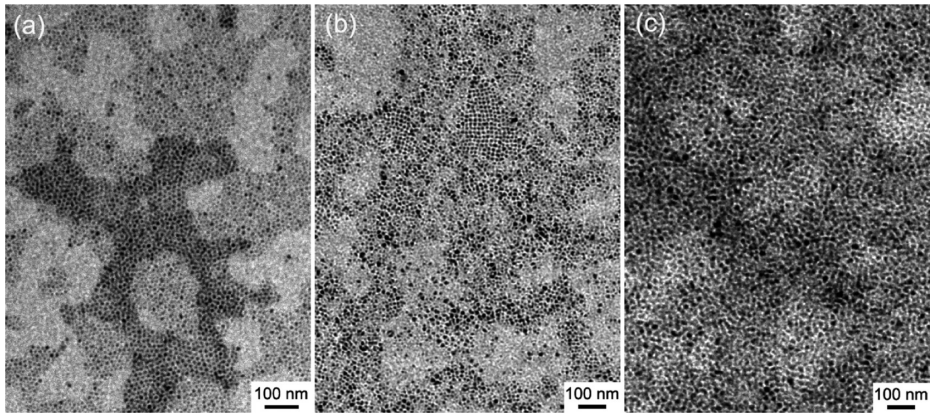

Figure 2. TEM images of (a) sample A, (b) sample B, and (c) sample C.

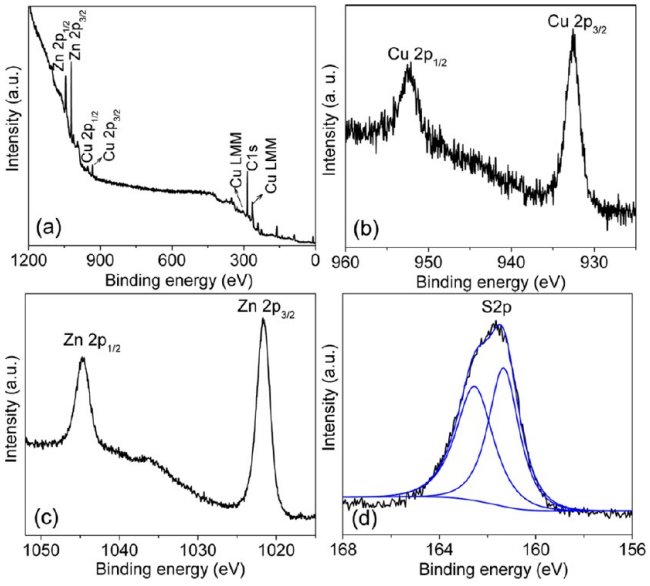

Figure 3. XPS spectra of the as-obtained sample C: (a) survey spectrum; (b) Cu 2p, (c) Zn 2p, and (d) S 2p.

(shown in Figure 3c) give a peak separation of 23.0 eV, consistent with the standard splitting of 22.97 eV, which suggests the presence of Zn^{2+} in the as-obtained samples.[40] The S 2p result shown in Figure 3d is fitted using a spin−orbit separation of 1.1 eV, and the two peaks are attributed to the S $2p_{3/2}$ and S $2p_{1/2}$, which may be due to the S ions coordinated to metal ions or the chemically bound thiolate sulfur.[41]

The UV−vis absorption spectra were employed to study the optical properties of the doped nanocrystals. Figure 4 shows absorption spectra of sample B and sample C obtained at 270 min. It can be seen that the absorption band at 276 nm appears in the absorption spectrum of sample B, and an obvious red-shift is observed in sample C. According to the above TEM results of sample B and C, the effect of particle size on the absorption peak can be neglected. As a result, the red-shift of absorption peak should be strongly associated with the doping levels of Cu^{+} ions in the lattice of ZnS particle matrix.[7]

Transformation from ZnS:Cu(I) Nanocrystals to $Cu_{1.94}S$−ZnS Heterostructured Nanocrystals. Different from our previous work about CdS:Cu(I) nanocrystals,[7] the as-obtained products are transformed from ZnS:Cu(I) nanocrystals to $Cu_{1.94}S$−ZnS heterostructured nanocrystals when the molar ratios of $Cu(acac)_2$ to $Zn(acac)_2$ is increased from

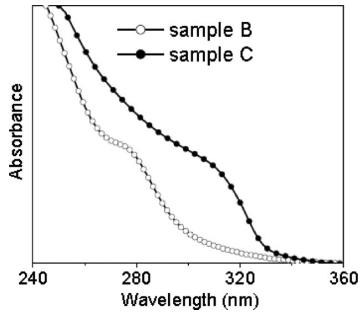

Figure 4. UV−vis absorption spectra of sample B and sample C obtained at 270 min.

1:9 to 3:7. Figure 5 depicts the XRD patterns and corresponding TEM images of samples D and E. As shown

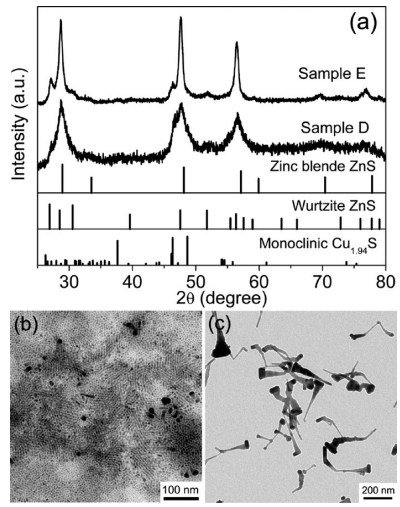

Figure 5. (a) XRD patterns of samples D and E together with the standard diffraction lines of zinc blende ZnS (JCPDS No. 80-0020), wurtzite ZnS (JCPDS No. 79-2204), and monoclinic $Cu_{1.94}S$ (JCPDS No. 23-0959).

in Figure 5a, the characteristic peaks of the cubic ZnS nanocrystals are observed in the XRD patterns of sample D, but some non-negligible diffraction peaks indexed to hexagonal wurtzite ZnS (JCPDS No. 79-2204) and monoclinic $Cu_{1.94}S$ (JCPDS No. 23-0959) are also observed. Correspondingly, the TEM image shown in Figure 5b indicates that the as-obtained

dx.doi.org/10.1021/la401707u | Langmuir 2013, 29, 8728−8735

product comprises vast majority of small doped nanocrystals and few heterostructured nanocrystals. As the reaction temperature is elevated to 270 °C, the diffraction peaks of wurtzite ZnS and monoclinic $Cu_{1.94}S$ become apparent in XRD patterns of sample E, and the widths of the three major peaks become narrower as compared to that of sample D, which suggests that particle size of sample E is larger than that of sample D. The TEM image shown in Figure 5c demonstrates that sample E is exclusively made up of taper-like heterostructured nanocrystals with oblate head and cone-shaped tail. This indicates that the increment of the reaction temperature leads to the formation of heterostructured nanocrystals in this work.

Further increasing the molar ratio of $Cu(acac)_2$ to $Zn(acac)_2$ results in the morphological variation of the as-obtained products. Figures 6a and 6b reveal the typical low-resolution

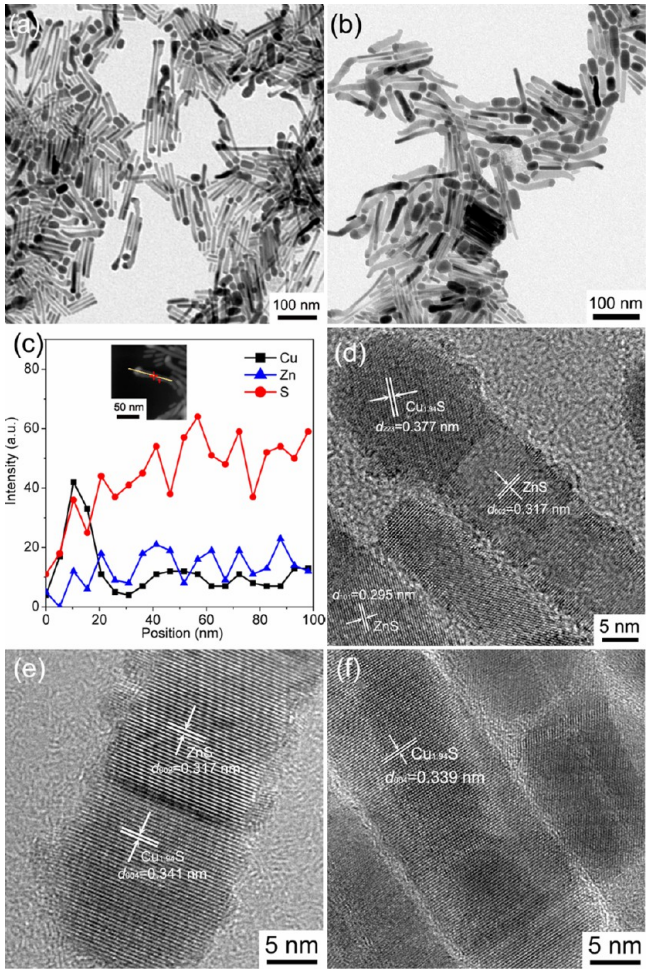

Figure 6. Low-resolution TEM images of sample F for (a) 180 min and (b) 360 min. (c) Elemental profiles of Cu, Zn, and S (the inset shows the high-angle annular dark-field scanning TEM image). (d, e) HRTEM images of two differently oriented heterostructured nanocrystals. (f) HRTEM image of $Cu_{1.94}S$ nanorods.

TEM images of sample F which were obtained at 180 and 360 min, respectively. As seen in Figure 6a, almost all the particles are composed of a quasi-spherical "head" and a slightly long "stick", and the mean length of the "tail" is about 118 nm and the mean diameter of the "head" is about 17 nm. Additionally, some isolated "heads" and "tails" are also present. As the reaction time is prolonged to 360 min, the morphology changes from matchstick-like to tadpole-shape with a crooked and relatively short "stick" (Figure 6b), but the mean diameter of the "head" is unchanged. The TEM images of sample F for different reaction time and the relationship between the length of "head" or "tail" versus reaction time are given in Figure S1 of the Supporting Information. The diameter of the "head" slightly changes while the length of the "tail" increases first but decreases afterward as the morphologiy evolves from match-stick-like shape to tadpole, which may be caused by the different binding strength of the Cu^+ and Zn^{2+} with the DDT.[42] Detailed analysis of the local elemental composition of the heterostructured nanocrystals was performed by line-scan energy-dispersive X-ray spectroscopy (Figure 6c). The elemental profiles demonstrate that Cu is dominant in the head and Zn in the stick part, while S is dispersed throughout the whole nanocrystals, which confirms the formation of $Cu_{1.94}S$–ZnS heterostructured nanocrystals. In order to provide more information about the interfacial structures of the heterostructured nanocrystals, HRTEM studies were further carried out. Figures 6d–f depict typical HRTEM images, in which the interface between two different materials within one particle is clearly observed. As shown in Figure 6d, the relatively dark region (the "head") is Cu-rich with a lattice spacing of 0.377 nm which can be ascribed to (223) planes of monoclinic $Cu_{1.94}S$, and the relatively bright region (the "stick") is Zn-rich with a interplanar distance of 0.317 nm, which can be indexed as the (002) plane of wurtzite ZnS. Also, the lattice fringes with an interplanar spacing of 0.295 nm are observed and can be ascribed to (101) plane of wurtzite ZnS. Furthermore, another analysis result of the lattice spacing shown in Figure 6e reveals that the $Cu_{1.94}S$ head interfaces epitaxially to the (002) plane of the ZnS "stick" through the (004) plane, suggesting that the grain boundary mainly consists of the (002) plane of ZnS and the plane (004) of $Cu_{1.94}S$ with a lattice mismatch of 7%. The HRTEM image (Figure 6e) also reveals that the (004) plane of $Cu_{1.94}S$ parallels to the plane (002) of ZnS. In addition, some short but thick nanorods are clearly observed in Figure 6a, and the corresponding HRTEM image is shown in Figure 6f; the obvious lattice fringes with a spacing of 0.339 nm can be observed, corresponding to the (004) plane of monoclinic $Cu_{1.94}S$, and thus the nanorod can be indexed as $Cu_{1.94}S$, which displays preferential growth along the [001] direction.

As mentioned above, the crystal-phase change of ZnS is accompanied by the transformation from doped nanocrystals to heterostructured nanocrystals. Figure 7 shows XRD patterns of sample F obtained at 360 min and sample G obtained at 180 and 360 min, respectively. The XRD pattern of sample F

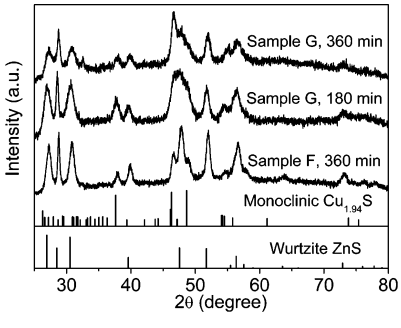

Figure 7. XRD patterns of sample F (360 min) and sample E (180 and 360 min).

dx.doi.org/10.1021/la401707u | *Langmuir* 2013, 29, 8728–8735

suggests a mixed phase of monoclinic $Cu_{1.94}S$ and wurtzite ZnS, and no impurities are detected. The strongest diffraction peak of ZnS phase corresponds to the (002) plane of hexagonal ZnS, and the long axis of the heterostructured nanocrystals can therefore be identified as *c*-axis of wurtzite ZnS.[20] As the molar ratio of $Cu(acac)_2$ to $Zn(acac)_2$ is further increased to be 7:3, monoclinic $Cu_{1.94}S$ and hexagonal ZnS could still be indexed from XRD patterns. As compared to that of sample F, the diffraction intensity of the characteristic peak corresponding to (080) plane of sample G obtained at 360 min becomes stronger, which implies that the proportion of monoclinic $Cu_{1.94}S$ phase increases in the heterostructured nanocrystals. Based on the XRD patterns of sample G obtained at 180 and 360 min, the characteristic diffraction peaks of $Cu_{1.94}S$ phase are more apparent in the product obtained at 180 min, suggesting that the crystal-phase changes from $Cu_{1.94}S$ to heterostructured nanocrystals with the increase of reaction time. Prior reports pointed out that $Cu_{1.94}S$ nanocrystals could be formed at first, and then ZnS phase could be formed from one tip of $Cu_{1.94}S$.[19,20] To further confirm the above proposition, the TEM images of the sample G at different reaction time are depicted in Figure 8. It can be seen that the majority of the products obtained at 30 min are spherical $Cu_{1.94}S$ nanocrystals, and then they disappear gradually until almost no isolated $Cu_{1.94}S$ nanospheres can be observed in the products obtained at 360 min. In contrast, the matchstick-shaped $Cu_{1.94}S$–ZnS heterostructured nanocrystals are dominant in the products obtained after 120 min, and the product obtained at 360 min exhibits an irregular-shaped "head" due to the Ostwald ripening process. The TEM results are in good agreement with the XRD results.

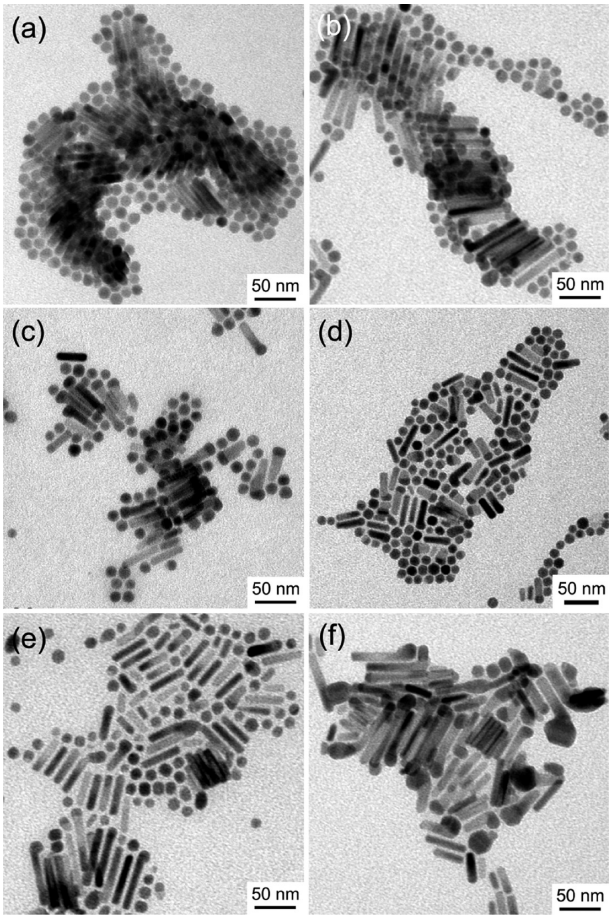

Figure 8. Low-resolution TEM images of sample G for different reaction time: (a) 30, (b) 70, (c) 120, (d) 180, (e) 270, and (f) 360 min.

A previous report illuminates that the transition metal ions prefer to be doped into cubic zinc blende host materials.[8] Generally, cubic ZnS nanocrystals are inclined to be formed by decomposition of Zn-DDT thiolate at a relatively high temperature.[35,43] Herein, cubic ZnS nanocrystals were synthesized successfully by direct heating $Zn(acac)_2$ in the mixture of DDT and ODE at 240 °C. Thus, the Cu^+ ions can be doped into the lattice of cubic ZnS nanocrystals when the molar ratio of $Cu(acac)_2$ to $Zn(acac)_2$ is kept less than 3:7. When the molar ratio of $Cu(acac)_2$ to $Zn(acac)_2$ is increased to exceed 5:5, hexagonal wurtzite ZnS is prone to be formed with the assistance of $Cu_{1.94}S$ nanocrystals. In this case, the doping process becomes more difficult; thus, the epitaxial growth becomes an alternative growth process. It is well-known that monoclinic $Cu_{1.94}S$ has high cationic mobility and thus has more cationic vacancies which benefits the dissolution of foreign anions.[19,28] Therefore, the growth evolution of heterostructured nanocrystals involves Zn^{2+} cations exchanging into $Cu_{1.94}S$ nanocrystals, and then the as-obtained product acts as a growing template for the formation of $Cu_{1.94}S$–ZnS heterostructured nanocrystals.[19]

Formation of Mixed Phase of $Cu_{1.81}S$ and $Cu_{1.8}S$ Nanocrystals. Further increasing the molar ratios of $Cu(acac)_2$ to $Zn(acac)_2$ to 9:1 does not result in heterostructured nanocrystals, but the mixed phase of cubic $Cu_{1.8}S$ and tetragonal $Cu_{1.81}S$ nanocrystals was obtained. It is noteworthy that the morphology changes from spherical to rice-shaped accompanied with the transformation of crystal-phase from $Cu_{1.94}S$ (djurleite) to the mixed phase of $Cu_{1.8}S$ and $Cu_{1.81}S$ (digenite). Figures 9a–d present TEM images of sample H obtained at different reaction time. As shown in Figure 9a, monodisperse spherical $Cu_{1.94}S$ nanocrystals with a mean size of 9.6 ± 0.7 nm is obtained at early 30 min. As the reaction time is prolonged to 70 min, some rice-shaped nanocrystals appear in the TEM image (Figure 9b). The corresponding XRD pattern shown in Figure 9f can be indexed as monoclinic djurleite $Cu_{1.94}S$, and the diffraction intensity of the (080) plane is the strongest. Further increasing the reaction time to 120 min, the amount of the rice-shaped nanocrystals is nearly equal with that of the spherical nanocrystals in the TEM image (Figure 9c), and ultimately the spherical nanocrystals have completely transformed into rice shape in the sample obtained at 270 min. The XRD pattern shown in Figure 9f suggests that it is a mixed phase of cubic $Cu_{1.8}S$ (JCPDS No. 09-0064) and tetragonal $Cu_{1.81}S$ (JCPDS No. 41-0959) rather than monoclinic $Cu_{1.94}S$. To the best of our knowledge, it is the first time to prepare the mixed phase of cubic $Cu_{1.8}S$ and tetragonal $Cu_{1.81}S$ nanocrystals using a simple wet-chemistry method. To gain more information on the product, a typical HRTEM image shown in Figure 9e reveals that the lattice fringes with an interplanar spacing of 0.308 nm can be indexed as the (842) plane of cubic $Cu_{1.8}S$, and the other lattice fringes with interplanar spacings of 0.330 and 0.324 nm, corresponding to (105) and (203) planes of tetragonal $Cu_{1.81}S$ phase, respectively. The obvious lattice fringes indicate the single crystalline structure and high crystallinity of the product. To further confirm the composition of the product, energy-dispersive X-ray (EDX) spectroscopy is performed to analyze

dx.doi.org/10.1021/la401707u | *Langmuir* 2013, 29, 8728–8735

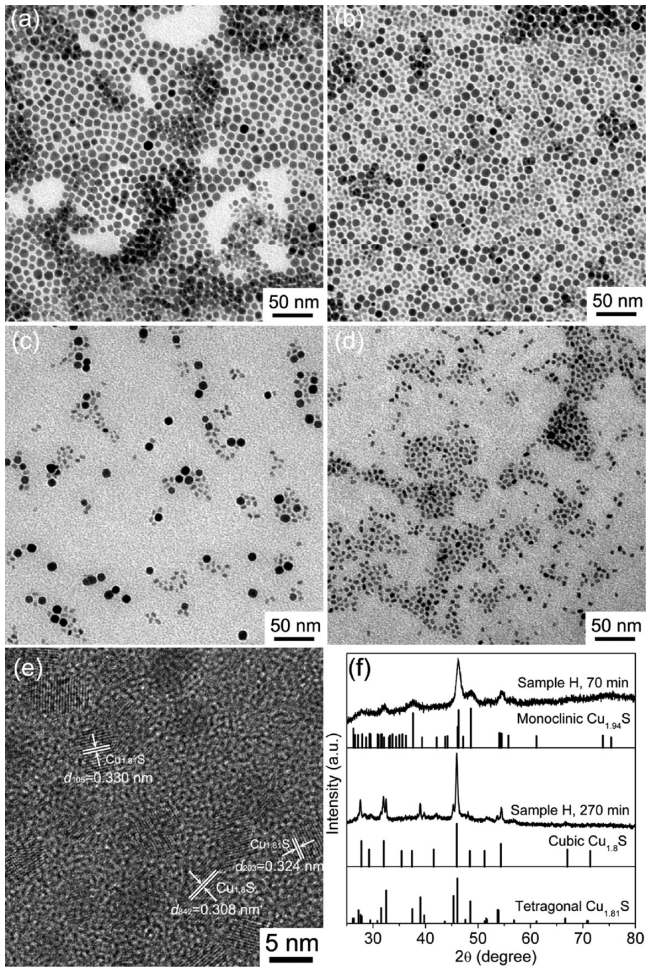

Figure 9. Low-resolution TEM images of sample H obtained for different reaction time: (a) 30, (b) 70, (c) 120, and (d) 270 min. (e) A typical HRTEM image of sample H. (f) XRD patterns of sample H obtained at 70 and 270 min, and the bottom lines are the standard diffraction lines of monoclinic $Cu_{1.94}S$ (JCPDS No. 23-0959), cubic $Cu_{1.8}S$ (JCPDS No. 09-0064), and tetragonal $Cu_{1.81}S$ (JCPDS No. 41-0959).

sample H obtained at 270 min which is dripped onto a carbon-coated nickel grid. The EDX result shown in Figure S2 of the Supporting Information demonstrates that both Zn and Cu elements are present in the product, and the atomic ratio of Cu to Zn is 4.6:1 (Table S1 of the Supporting Information), which suggests that Zn is incorporated into $Cu_{1.94}S$ matrix. The incorporation of Zn^{2+} into $Cu_{1.94}S$ lattices to replace some Cu^{+} results in the crystal-phase transformation from monoclinic djurleite $Cu_{1.94}S$ to mixed-crystalline structure composed of $Cu_{1.8}S$ and $Cu_{1.81}S$.[12] During this reaction, the decomposition of the Cu−thiolate compound into $Cu_{1.94}S$ nanocrystals is easier than that of the Zn−thiolate compound that requires a relatively high temperature; thus, the $Cu_{1.94}S$ nanocrystals are first formed.[35] It is stated previously that monoclinic $Cu_{1.94}S$ has high cationic mobility, and the copper ions have no special positions but move through the whole available space.[28,44] Therefore, once the decomposition of Zn−thiolate compound startes, free Zn^{2+} may be doped into $Cu_{1.94}S$ lattice in place of Cu ions and made the Cu ions out of the crystal lattice, leading to the phase transformation.[45] Further investigation about the phase transformation is under way.

Recently, $Cu_{1.94}S$ nanocrystals have been reported to exhibit localized surface plasmon resonance (LSPR) in the near-infrared (NIR) region from excess holes in the valence band due to Cu deficiencies; thus, LSPR spectroscopy can be used to profile the stoichiometry and phase of doped nanocrystals.[46,47] To further study the effects of the incorporation of Zn^{2+} into $Cu_{1.94}S$ lattices on the absorption spectra of the as-obtained products, the UV−vis−NIR absorption spectra of sample H for different reaction time have been measured in chloroform, which are shown in Figure 10. For the products obtained at 30,

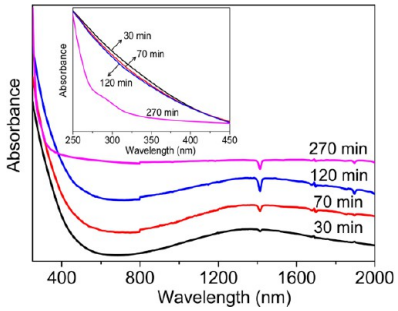

Figure 10. Absorption spectra of sample H for different reaction time, which were measured in choloroform, and the inset shows the absorption spectra in the region from 250 to 450 nm.

70, and 120 min, LSPR peaks in the NIR region can be clearly observed, but the LSPR intensity becomes relatively weaker for the product obtained at 120 min. In addition, as the phase transforms from $Cu_{1.94}S$ to mixed phase composed of $Cu_{1.8}S$ and $Cu_{1.81}S$, the absorption band in the NIR region disappears, but an absorption band in the region from 275 to 310 nm is observed from the product obtained at 270 min (the inset of Figure 10), indicating the absence of the LSPR mode in the NIR region due to the incorporation of Zn^{2+} into $Cu_{1.94}S$ lattice to minimize the Cu vacancies.[46] Unfortunately, at this stage, we cannot conclude the genuine reason for the result, and further investigation is going on.

4. CONCLUSIONS

In summary, different Cu−Zn−S-based nanocrystals including ZnS:Cu(I), $Cu_{1.94}S$−ZnS heterostructures, and mixed phase composed of $Cu_{1.8}S$ and $Cu_{1.81}S$ (digenite) have been synthesized using a simple one-pot method, which involves the thermal decomposition of $Cu(acac)_2$ and $Zn(acac)_2$ in the mixture of DDT and ODE at a relatively high temperature. The transformation of chemical composition can be achieved just by adjusting the molar ratios of $Cu(acac)_2$ to $Zn(acac)_2$ accompanied with crystal-phase changing from cubic ZnS to hexagonal ZnS. The morphology of the products can be tuned in the form of taper-like, matchstick-like, tadpole-like, and rice-shaped by changing reaction time, reaction temperature, and the precursor ratios. This one-pot synthetic procedure is simple and highly reproducible, which provides a facile approach to produce unique doped or heterostructured semiconductor nanocrystals with multifunctional properties for application in optoelectronic devices in the near future.

■ ASSOCIATED CONTENT

Supporting Information

TEM image of sample F for different reaction times and the EDX results of sample H. This material is available free of charge via the Internet at http://pubs.acs.org.

dx.doi.org/10.1021/la401707u | Langmuir 2013, 29, 8728−8735

AUTHOR INFORMATION

Corresponding Author

*Tel +86 10 51683627, e-mail awtang@bjtu.edu.cn (A.T.); Tel +86 10 51684860, e-mail fteng@bjtu.edu.cn (F.T.).

Notes

The authors declare no competing financial interest.

ACKNOWLEDGMENTS

This work was partly supported by the National Natural Science Foundation of China (61108063), the National Science Foundation for Distinguished Young Scholars of China (61125505), and Basic Scientific Research Fund of Beijing JiaoTong University (2013JBZ004, 2010JBZ006), and A.W. is also grateful for the financial support from Beijing JiaoTong University (2011JBM301, 2012RC046).

REFERENCES

(1) Sun, Q. J.; Wang, Y. A.; Li, L. S.; Wang, D. Y.; Zhu, T.; Xu, J.; Yang, C. H.; Li, Y. F. Bright, multicoloured light-emitting diodes based on quantum dots. *Nat. Photonics* **2007**, *1*, 717−722.

(2) Qian, L.; Zheng, Y.; Xue, J. G.; Holloway, P. H. Stable and efficient quantum-dot light-emitting diodes based on solution-processed multilayer structures. *Nat. Photonics* **2011**, *5*, 543−548.

(3) Yang, J. H.; Tang, A. W.; Zhou, R. J.; Xue, J. G. Effects of nanocrystal size and device aging on performance of hybrid poly(3-hexylthiophene):CdSe nanocrystal solar cells. *Sol. Energy Mater. Sol. Cells* **2011**, *95*, 476−482.

(4) Qian, L.; Yang, J. H.; Zhou, R. J.; Tang, A. W.; Zheng, Y.; Tseng, T. K.; Bera, D.; Xue, J. G.; Holloway, P. H. Hybrid polymer-CdSe solar cells with a ZnO nanoparticle buffer layer for improved efficiency and lifetime. *J. Mater. Chem.* **2011**, *21*, 3814−3817.

(5) Hu, F. Q.; Ran, Y. L.; Zhou, Z.; Gao, M. Y. Preparation of bioconjugates of CdTe nanocrystals for cancer marker detection. *Nanotechnology* **2006**, *17*, 2972−2977.

(6) Zhou, Y. L.; Zhu, Z. N.; Huang, W. X.; Liu, W. J.; Wu, S. J.; Liu, X. F.; Gao, Y.; Zhang, W.; Tang, Z. Y. Optical coupling between chiral biomolecules and semiconductor nanoparticles: Size-dependent circular dichroism absorption. *Angew. Chem., Int. Ed.* **2011**, *50*, 11456−11459.

(7) Tang, A. W.; Yi, L. X.; Han, W.; Teng, F.; Wang, Y. S.; Hou, Y. B.; Gao, M. Y. Synthesis, optical properties and superlattice structure of Cu(I)-doped CdS nanocrystals. *Appl. Phys. Lett.* **2010**, *97*, 033112.

(8) Srivastava, B. B.; Jana, S.; Pradhan, N. Doping Cu in semiconductor nanocrystals: some old and some new physical insights. *J. Am. Chem. Soc.* **2011**, *133*, 1007−1015.

(9) Wang, Y.; Hou, Y. B.; Tang, A. W.; Feng, B.; Li, Y.; Liu, J.; Teng, F. Synthesis and optical properties of composition-tunable and water-soluble $Zn_xCd_{1-x}Te$ alloyed nanocrystals. *J. Cryst. Growth* **2007**, *308*, 19−25.

(10) Li, Y. C.; Ye, M. F.; Yang, C. H.; Li, X. H.; Li, Y. F. Composition- and shape-controlled synthesis and optical properties of $Zn_xCd_{1-x}S$ alloyed nanocrystals. *Adv. Funct. Mater.* **2005**, *15*, 433−441.

(11) Carbone, L.; Cozzoli, P. D. Colloidal heterostructured nanocrystals: Synthesis and growth mechanisms. *Nano Today* **2010**, *5*, 449−493.

(12) Han, W.; Yi, L. X.; Zhao, N.; Tang, A. W.; Gao, M. Y.; Tang, Z. Y. Synthesis and shape-tailoring of the copper sulfide/indium sulfide-based nanocrystals. *J. Am. Chem. Soc.* **2008**, *130*, 13152−13161.

(13) Pradhan, N.; Peng, X. G. Efficient and color-tunable Mn-doped ZnSe nanocrystal emitters: Control of optical performance via greener synthetic chemistry. *J. Am. Chem. Soc.* **2007**, *129*, 3339−3347.

(14) Pradhan, N.; Sarma, D. D. Advances in light-emitting doped semiconductor nanocrystals. *J. Phys. Chem. Lett.* **2011**, *2*, 2818−2826.

(15) Erwin, S. C.; Zu, L. J.; Haftel, M. I.; Efros, A. L.; Kennedy, T. A.; Norris, D. J. Doping semiconductor nanocrystals. *Nature* **2005**, *436*, 91−94.

(16) Quan, Z. W.; Yang, D. M.; Li, C. X.; Kong, D. Y.; Yang, P. P.; Cheng, Z. Y.; Lin, J. Multicolor tuning of manganese-doped ZnS colloidal nanocrystals. *Langmuir* **2009**, *25*, 10259−10262.

(17) Cho, S.; Jang, J.-W.; Kim, J.; Lee, J. S.; Choi, W.; Lee, K.-H. Three-dimensional type II ZnO/ZnSe heterostructures and their visible light photocatalytic activities. *Langmuir* **2011**, *27*, 10243−10250.

(18) Shen, S. L.; Zhang, Y. J.; Peng, L.; Du, Y. P.; Wang, Q. B. Matchstick-shaped Ag_2S−ZnS heteronanostructures preserving both UV/blue and near-infrared photoluminescence. *Angew. Chem.* **2011**, *123*, 7253−7256.

(19) Han, S. K.; Gong, M.; Yao, H. B.; Wang, Z. M.; Yu, S. H. One-pot controlled synthesis of hexagonal-prismatic $Cu_{1.94}S$-ZnS, $Cu_{1.94}S$-ZnS-$Cu_{1.94}S$, and $Cu_{1.94}S$-ZnS-$Cu_{1.94}S$-ZnS-$Cu_{1.94}S$ heteronanostructures. *Angew. Chem., Int. Ed.* **2012**, *51*, 6365−6368.

(20) Yi, L. X.; Tang, A. W.; Niu, M.; Han, W.; Hou, Y. B.; Gao, M. Y. Synthesis and self-assembly of $Cu_{1.94}S$-ZnS heterostructured nanorods. *CrystEngComm* **2010**, *12*, 4124−4130.

(21) Huang, F.; Wang, X. L.; Xu, J.; Chen, D. Q.; Wang, Y. S. A plasmonic nano-antenna with controllable resonance frequency: $Cu_{1.94}S$−ZnS dimeric nanoheterostructure synthesized in solution. *J. Mater. Chem.* **2012**, *22*, 22614−22618.

(22) Yi, L. X.; Liu, Y. Y.; Yang, N. L.; Tang, Z. Y.; Zhao, H. J.; Ma, G. H.; Su, Z. G.; Wang, D. One dimensional $CuInS_2$−ZnS heterostructured nanomaterials as low-cost and high-performance counter electrodes of dye-sensitized solar cells. *Energy Environ. Sci.* **2013**, *6*, 835−840.

(23) Tang, A. W.; Teng, F.; Wang, Y.; Hou, Y. B.; Han, W.; Yi, L. X.; Gao, M. Y. Polymer/nanocrystal photovoltaic devices based on matchstick-like Cu_2S−In_2S_3 heterostructure nanocrystals. *Nanoscale Res. Lett.* **2008**, *3*, 502−507.

(24) Depalo, N.; Carrieri, P.; Comparelli, R.; Striccoli, M.; Agostiano, A.; Bertinetti, L.; Innocenti, C.; Sangregorio, C.; Curri, M. L. Biofunctionalization of anisotropic nanocrystalline semiconductor−magnetic heterostructures. *Langmuir* **2011**, *27*, 6962−6970.

(25) Demchenko, D. O.; Robinson, R. D.; Sadtler, B.; Ergonmez, C. K.; Alivisatos, A. P.; Wang, L. W. Formation mechanism and properties of CdS-Ag_2S nanorod superlattices. *ACS Nano* **2008**, *2*, 627−636.

(26) Cozzoli, P. D.; Pellegrino, T.; Manna, L. Synthesis, properties and perspectives of hybrid nanocrystal structures. *Chem. Soc. Rev.* **2006**, *35*, 1195−1208.

(27) Feng, X. M.; Hu, G. Q.; Hu, J. Q. Solution-phase synthesis of metal and/or semiconductor homojunction/heterojunction nanomaterials. *Nanoscale* **2011**, *3*, 2099−2117.

(28) Zhu, G. X.; Xu, Z. Controllable growth of semiconductor heterostructures mediated by bifunctional Ag_2S nanocrystals as catalyst or source-host. *J. Am. Chem. Soc.* **2011**, *133*, 148−157.

(29) Liao, H. C.; Jao, M. H.; Shyue, J. J.; Chen, Y. F.; Su, W. F. Facile synthesis of wurtzite copper−zinc−tin sulfide nanocrystals from plasmonic djurleite nuclei. *J. Mater. Chem., A* **2013**, *1*, 337−341.

(30) Murray, C. B.; Norris, D. J.; Bawendi, M. G. Synthesis and characterization of nearly monodisperse CdE (E = sulfur, selenium, tellurium) semiconductor nanocrystallites. *J. Am. Chem. Soc.* **1993**, *115*, 8706−8715.

(31) Pradhan, N.; Goorskey, D.; Thessing, J.; Peng, X. G. An alternative of CdSe nanocrystal emitters: Pure and tunable Impurity emissions in ZnSe nanocrystals. *J. Am. Chem. Soc.* **2005**, *127*, 17586−17587.

(32) Zhong, W. J.; Li, Y.; Zhang, H.; Zhou, X. G.; Zhong, X. H. Facile synthesis of ZnS-$CuInS_2$ alloyed nanocrystals for a color-tunable fluorchrome and photocatalyst. *Inorg. Chem.* **2011**, *50*, 10432−10438.

(33) Milliron, D. J.; Hughes, S. M.; Cui, Y.; Manna, L.; Li, J. B.; Wang, L. W.; Alivisatos, A. P. Colloidal nanocrystal heterostructures with linear and branched topology. *Nature* **2004**, *430*, 190−195.

(34) Sugunan, A.; Zhao, Y. C.; Mitra, S.; Dong, L.; Li, S. H.; Popov, S.; Marcinkevicius, S.; Toprak, M. S.; Muhammed, M. Synthesis of tetrahedral quasi-type-II CdSe-CdS core-shell quantum dots. *Nanotechnology* **2011**, *22*, 425202.

(35) Zhuang, Z. B.; Lu, X. T.; Peng, Q.; Li, Y. D. A facile "dispersion-decomposition" route to metal sulfide nanocrystals. *Chem.—Eur. J.* **2011**, *17*, 10445−10452.
(36) Regulacio, M. D.; Ye, C.; Lim, S. H.; Bosman, M.; Polavarapu, L.; Koh, W. L.; Zhang, J.; Xu, Q. H.; Han, M. Y. One-pot synthesis of $Cu_{1.94}S$−CdS and $Cu_{1.94}S$-$Zn_xCd_{1-x}S$ nanodisk heterostructures. *J. Am. Chem. Soc.* **2011**, *133*, 2052−2055.
(37) Zhuang, T. T.; Fan, F. J.; Gong, M.; Yu, S. H. $Cu_{1.94}S$ nanocrystal seed mediated solution-phase growth of unique Cu_2S−PbS heteronanostructures. *Chem. Commun.* **2012**, *48*, 9762−9764.
(38) Meulenberg, R. W.; Buuren, T.; van Hanif, K. M.; Willey, T. M.; Stouse, G. F.; Terminello, L. J. Structure and composition of Cu-doped CdSe nanocrystals using soft X-ray absorption spectroscopy. *Nano Lett.* **2004**, *4*, 2277−2285.
(39) Li, S.; Wang, H. Z.; Lu, W. W.; Si, H. L.; Tao, X. J.; Lou, S. Y.; Du, Z. L.; Li, L. S. Synthesis and assembly of monodisperse spherical Cu_2S nanocrystals. *J. Colloid Interface Sci.* **2009**, *330*, 483−487.
(40) Wang, J. J.; Hu, J. S.; Guo, Y. G.; Wan, L. J. Wurtzite $Cu_2ZnSnSe_4$ nanocrystals for high-performance organic−inorganic hybrid photodetectors. *NPG Asia Mater.* **2012**, *4*, e2.
(41) Tang, A. W.; Qu, S. C.; Li, K.; Hou, Y. B.; Teng, F.; Cao, J.; Wang, Y. S.; Wang, Z. G. One-pot synthesis and self-assembly of colloidal copper(I) sulfide nanocrystals. *Nanotechnology* **2010**, *21*, 285602.
(42) Wang, Y-H. A.; Zhang, X. Y.; Bao, N. Z.; Lin, B. P.; Gupta, A. Synthesis of shape-controlled monodisperse wurtzite $CuIn_xGa_{1-x}S_2$ semiconductor nanocrystals with tunable band gap. *J. Am. Chem. Soc.* **2011**, *133*, 11072−11075.
(43) Choi, S.-H.; An, K.; Kim, E.-G.; Yu, J. H.; Kim, J. H.; Hyeon, T. Simple and generalized synthesis of semiconducting metal sulfide nanocrystals. *Adv. Funct. Mater.* **2009**, *19*, 1645−1649.
(44) Okamoto, K.; Kawai, S. Electrical conduction and phase transition of copper sulfides. *Jpn. J. Appl. Phys.* **1973**, *12*, 1130−1138.
(45) Lotfipour, M.; Machani, T.; Rossi, D. P.; Plass, K. E. α-Chalcocite nanoparticle synthesis and stability. *Chem. Mater.* **2011**, *23*, 3032−3038.
(46) Luther, J. M.; Jaih, P. K.; Ewers, T.; Alivisatos, A. P. Localized surface plasmon resonances arising from free carriers in doped quantum dots. *Nat. Mater.* **2011**, *10*, 361−366.
(47) Hsu, S. W.; On, K.; Tao, A. R. Localized surface plasmon resonances of anisotropic semiconductor nanocrystals. *J. Am. Chem. Soc.* **2011**, *133*, 19072−19075.